2024 Tenth Indian Control Conference (ICC)
9 - 11 December, 2024
IISER Bhopal, India

Robust Stabilization of a Knee Exoskeleton Robot using an LMI-based Composite Controller

Sahar Jenhani[1], Hassène Gritli[2] and Jyotindra Narayan[3]

Abstract— **Rehabilitation exoskeleton robots are vital for restoring lower limb functionality in individuals with locomotor disorders. Extensive research has focused on optimizing the control of these robotic systems and make them more stable. However, there is still a considerable gap in developing robust controllers. This work introduces a robust control approach tailored for a one-degree-of-freedom (1-DoF) knee rehabilitation exoskeleton robot. Emphasizing position control, our method addresses challenges such as parameter uncertainties, solid and viscous frictions, external disturbances, and motion constraints. To effectively manage these issues, we propose a composite controller that integrates a linear state-feedback controller and a nonlinear control law. By employing a quadratic Lyapunov function, we derive the expression of the nonlinear controller and establish the LMI conditions required for calculating the matrix gain of the composite controller using two different design methods. To confirm the developed LMI conditions and demonstrate the proposed control method's ability to ensure robust position control of the knee exoskeleton robotic system, simulation results are finally provided.**

I. Introduction

Rehabilitation exoskeletons offer efficient, personalized alternatives to traditional methods by augmenting or restoring physical capabilities through strength amplification, mechanical support, and motion support. Applications in physical therapy, mobility aid, and rehabilitation are drawing interest [1]–[3]. By offering both everyday activity assistance and exercise training, these devices fill the void that exists between therapeutic treatments and assistive technology [4]. Their effectiveness depends heavily on control systems [1]–[3], which ensure safe and effective operation by enhancing adaptability, stability, and user safety. For exoskeleton motions to precisely support, magnify, or restore human movements, control algorithms are therefore needed.

In recent years, research has specifically focused on controlling exoskeleton knee devices for total knee rehabilitation in individuals with spinal cord injuries [5]–[8]. Motorized orthoses are utilized for this purpose, employing control mechanisms to address friction or gravity forces, ensuring gait rehabilitation, stabilizing body posture, and regulating leg trajectory [9]–[12]. Development efforts have targeted exoskeletons with 1-DoF to reduce the size, weight, and electrical equipment requirements for targeted movement support or therapy [7]. In [13], a state-feedback controller was designed to regulate a 1-DoF lower limb orthosis at the knee joint level, providing a robust solution for position control. Furthermore, authors in [14] introduced a composite controller combining linear state-feedback and nonlinear control to enhance stability under nonlinear conditions. However, these works did not account for state constraints, which are crucial in ensuring safe and stable operation under practical conditions.

To address the benchmark problem outlined above, this paper focuses on controlling a 1-DoF joint exoskeleton orthosis. This work introduces a nonlinear composite controller specifically designed to manage the complex nonlinear dynamics of the knee-joint exoskeleton in the presence of parameter uncertainties, external disturbances, and motion constraints. To effectively tackle these challenges, we approximate the nonlinear function inherent in the robot dynamics and constrain it within the bounds of a linear equation. The adopted controller consists of two main components: a linear component, represented by the state-feedback control law formulated through the Lyapunov approach, and a nonlinear component aimed at mitigating the effects of external disturbances and frictions. We define the conditions on the feedback gain of the control law as LMIs, guaranteeing the stabilization of the closed-loop system, by employing two distinct design approaches. To verify the designed conditions and assess the effectiveness of the suggested composite control law, simulation results are finally given.

The structure of the paper is as follows: Section II introduces the dynamics of the exoskeleton robotic system. Section III covers the regulated dynamics utilizing the proposed control law. In Section IV, we derive the LMI conditions necessary for the control law gains. Simulation results are presented in Section V. The work is concluded in Section VI, which also suggests possible further research.

II. Dynamics of the Knee Exoskeleton

A. System Overview

This work investigates wearable exoskeletons operating in the sagittal plane that have 1 to 3 degrees of freedom (DoF) per leg. These exoskeletons may feature joints that are passive, active, or fixed. Our focus is on the precise position control of a powered lower-limb exoskeleton, particularly targeting the knee joint [7], [15], [16]. Specifically, 1-DoF exoskeletons are tailored for scenarios requiring support or

[1]Sahar Jenhani is with the Laboratory of Robotics, Informatics and Complex Systems (RISC Lab - LR16ES07), National Engineering School of Tunis, University of Tunis El Manar, Le Belvédère, 1002, Tunis, Tunisia saharjenhani1@hotmail.com

[2]Hassène Gritli is with the Higher Institute of Information and Communication Technologies, University of Carthage, Borj Cedria, 1164, Tunis, Tunisia. He is also with the RISC Lab. grhass@yahoo.fr ; hassene.gritli@istic.ucar.tn

[3]Jyotindra Narayan is with the Department of Mechanical Engineering, Thapar Institute of Engineering and Technology, Patiala, 147004, Punjab, India. He is also with the Department of Computing, Imperial College London, UK. n.jyotindra@gmail.com

rehabilitation of a single movement aspect [7], [8], [17]–[19]. The exoskeleton orthosis, illustrated in Fig. 1, has a 1-DoF knee joint, chosen for its straightforward design and alignment with our research objectives. This design is particularly advantageous for individuals with knee joint impairments, offering simplicity and ease of use [7].

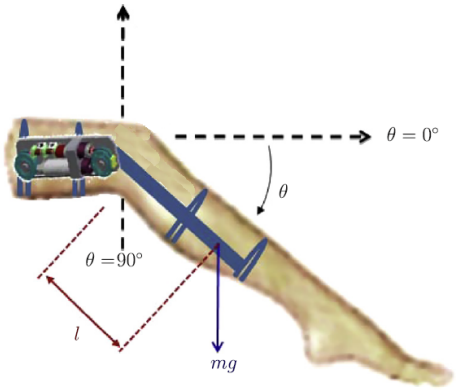


Fig. 1. Depiction of the actuated knee exoskeleton robot [7], [12].

B. Nonlinear Dynamic Modeling

To address the complexities of the knee exoskeleton's behavior, including uncertainties from unmodeled dynamics, parameter variations, and external disturbances, we developed a detailed nonlinear dynamic model. This model takes parameter uncertainties and external disturbances like viscous and solid frictions into account. The following is the formulation of the equation that controls the nonlinear motion of the knee exoskeleton seen in Fig. 1:

$$\vartheta\ddot{\theta} = u - f_v\dot{\theta} + a\cos(\theta) - f_s\text{sgn}(\dot{\theta}) + \delta_t \tag{1}$$

In this equation, ϑ denotes the inertia of the exoskeleton, f_v represents the viscous friction coefficient, f_s symbolizes the solid friction coefficient, and δ_t denotes the load torque. Additionally, $a = mgl$, where m is the mass of the exoskeleton, l is its length, and g is the acceleration due to gravity.

We decompose the dynamic model into nominal and uncertain parts, with the parameters defined as:

$$\begin{aligned} a &= a_\star + \Delta a & \vartheta &= \vartheta_\star + \Delta\vartheta \\ f_v &= f_v^\star + \Delta f_v & f_s &= f_s^\star + \Delta f_s \end{aligned} \tag{2}$$

By substituting these parameters into the nonlinear dynamics equation (1), we derive the following dynamic model:

$$\vartheta_\star\ddot{\theta} = -f_s^\star\text{sgn}(\dot{\theta}) - f_v^\star\dot{\theta} + a_\star\cos(\theta) + u + \Delta_t \tag{3}$$

Here, Δ_t represents the total disturbance, expressed as:

$$\Delta_t = \delta_t - \Delta\vartheta\ddot{\theta} + \Delta a\cos(\theta) - \Delta f_s\text{sgn}(\dot{\theta}) - \Delta f_v\dot{\theta} \tag{4}$$

To address the complexities of the system dynamics, we define Δ_t as the total disturbance, assuming it to be bounded by $\bar{\delta}$. This assumption is common in control theory and ensures system stability and robustness while encompassing various uncertainties, including parameter variations and external influences. Therefore, we assume that Δ_t meets the following constraint:

$$|\Delta_t| \leq \bar{\delta}, \qquad \bar{\delta} > 0 \tag{5}$$

Defining $\phi = \theta - \theta_d$, where θ_d is the intended position for controlling the exoskeleton robotic system, and considering $\dot{\theta} = \dot{\phi}$ and $\ddot{\theta} = \ddot{\phi}$, we can rewrite the dynamics (3) as:

$$\vartheta_\star\ddot{\phi} = -f_s^\star\text{sgn}(\dot{\phi}) - f_v^\star\dot{\phi} + a_\star\cos(\phi + \theta_d) + u + \Delta_t \tag{6}$$

C. Control Effort Calculation

The knee exoskeleton robot requires constant control effort to keep it in balance ($\dot{\theta}_d = 0$) and at the appropriate angle θ_d. Let u_d be the control effort required at equilibrium. Using equation (1), the desired control u_d is derived as:

$$u_d = -a_\star\cos(\theta_d) \tag{7}$$

III. Designing the Composite Controller

A. Problem Formulation

This study focuses on a knee rehabilitation exoskeleton robot, which operates within a range of 90°, as shown in Fig. 1. Here, 0° represents full knee extension, and 90° indicates the resting position. The operational range Ω is defined as:

$$\Omega = \{\theta \in \mathbb{R} : 0 \leq \theta \leq \frac{\pi}{2}\} \tag{8}$$

B. State Space Representation

Given $\phi = \theta - \theta_d$ and considering the state constraint in (8), the following relationship can be established:

$$-\sigma_{31} \leq \phi \leq \sigma_{32} \tag{9}$$

where $\sigma_{31} = \theta_d$ and $\sigma_{32} = \frac{\pi}{2} - \theta_d$.

Let $z = \begin{bmatrix} \phi & \dot{\phi} \end{bmatrix}^{\text{T}}$ be defined as the state vector. Rewriting the motion equation (6) yields the following:

$$\begin{aligned} \dot{z} =& \mathcal{A}z + \mathcal{B}u + \mathcal{D}_1\Phi_1(z) + \mathcal{D}_2\Phi_2(z) + \mathcal{B}\Delta_t \\ \text{with} \quad & -\sigma_{31} \leq \mathcal{C}^{\text{T}}z \leq \sigma_{32} \end{aligned} \tag{10}$$

where $\Phi_1(z)$ and $\Phi_2(z)$ are defined as follows:

$$\Phi_1(z) = \text{sgn}(\dot{\phi}) \qquad \Phi_2(z) = \cos(\phi + \theta_d) \tag{11}$$

The matrices $\mathcal{A}$, $\mathcal{B}$, $\mathcal{D}_1$, $\mathcal{D}_2$ and $\mathcal{C}$ are given like so:

$$\begin{aligned} \mathcal{A} &= \begin{bmatrix} 0 & 1 \\ 0 & -\frac{f_v^\star}{\vartheta_\star} \end{bmatrix} \quad \mathcal{B} = \begin{bmatrix} 0 \\ \frac{1}{\vartheta_\star} \end{bmatrix} \quad \mathcal{D}_1 = \begin{bmatrix} 0 \\ -\frac{f_s^\star}{\vartheta_\star} \end{bmatrix} \\ \mathcal{D}_2 &= \begin{bmatrix} 0 \\ \frac{a_\star}{\vartheta_\star} \end{bmatrix} \qquad \mathcal{C} = \begin{bmatrix} 1 \\ 0 \end{bmatrix} \end{aligned} \tag{12}$$

C. Composite Controller Strategy

Our objective is to regulate and stabilize the knee exoskeleton at a specified position θ_d. To achieve this, we propose a composite controller described as follows:

$$u = u_{nl} + u_l \tag{13}$$

where u_l denotes the linear state-feedback controller:

$$u_l = u_d + \Delta u_l \tag{14}$$

with u_d is determined via (7), and the adjustment term Δu_l is defined like so:

$$\Delta u_l = \begin{cases} \mathcal{K}z & \text{if} \quad \|z\|^2 \geq \epsilon^2 \\ 0 & \text{if} \quad \|z\|^2 < \epsilon^2 \end{cases} \tag{15}$$

where $\mathcal{K}$ indicates the gains matrix that will be created after, and the parameter ϵ represents a sufficiently small constant, which will be determined later.

Furthermore, the proposed controller (13) combines a nonlinear control law (u_{nl}) with a linear state-feedback controller (u_l). The linear control law, derived using the LMI technique, ensures stability, while the nonlinear controller addresses external disturbances and frictional effects.

Remark 1: The control design adopted in this study considers that the linear state-feedback control law u_l is set to zero when $\|z\|^2 < \epsilon^2$. It is important to note that this constraint is adopted only for the second design approach to address issues arising from the LMI development. However, the nonlinear control law u_{nl} remains active in this regime, effectively managing the system's dynamics and ensuring stability. This nonlinear controller is specifically designed to compensate for disturbances, providing a robust control strategy across the entire operating range.

D. Dynamics Under the Composite Controller

Upon integrating the composite controller (13) into the system dynamics (10), the resulting closed-loop model is expressed as:

$$\begin{aligned} &\dot{z} = (\mathcal{A} + \mathcal{B}\mathcal{K})\, z + \mathcal{B}\; u_{nl} + \mathcal{D}_1\Phi_1(z) + \mathcal{D}_2\Phi_3(z) + \mathcal{B}\Delta_t \\ &\text{such that} \quad -\sigma_{31} \leq \mathcal{C}^{\mathrm{T}} z \leq \sigma_{32} \quad \text{and} \quad \|z\|^2 \geq \epsilon^2 \end{aligned} \tag{16}$$

The function $\Phi_3(z)$ is defined like so:

$$\Phi_3(z) = -\cos(\theta_d) + \cos(\phi + \theta_d) \tag{17}$$

IV. Synthesis of the Nonlinear Controller and LMI Conditions

A. Nonlinear Controller Design

Let us consider the following candidate Lyapunov function allowing to guide the development of the nonlinear controller:

$$\begin{aligned} &\mathcal{V}(z) = z^{\mathrm{T}}\mathcal{P}z > 0 \quad \text{such that} \quad -\sigma_{31} \leq \mathcal{C}^{\mathrm{T}} z \leq \sigma_{32} \\ &\text{and} \quad \|z\|^2 \geq \epsilon^2 \end{aligned} \tag{18}$$

The time derivative of $\mathcal{V}(z)$ yields:

$$\begin{aligned} &\dot{\mathcal{V}}(z) = \dot{z}^{\mathrm{T}}\mathcal{P}z + z^{\mathrm{T}}\mathcal{P}\dot{z} < 0 \quad \text{such that} \\ &-\sigma_{31} \leq \mathcal{C}^{\mathrm{T}} z \leq \sigma_{32} \quad \text{and} \quad \|z\|^2 \geq \epsilon^2 \end{aligned} \tag{19}$$

Since $\mathcal{P} = \mathcal{P}^{\mathrm{T}} > 0$, we can rewrite expression (19) as:

$$\begin{aligned} \dot{\mathcal{V}}(z) = 2z^{\mathrm{T}}\mathcal{P}\dot{z} < 0 \;\; &\text{such that} \; -\sigma_{31} \leq \mathcal{C}^{\mathrm{T}} z \leq \sigma_{32} \\ &\text{and} \;\; \|z\|^2 \geq \epsilon^2 \end{aligned} \tag{20}$$

Utilizing (16), we express the time derivative as:

$$\begin{aligned} \dot{\mathcal{V}}(z) =& 2z^{\mathrm{T}}\mathcal{P}\left(\mathcal{A} + \mathcal{B}\mathcal{K}\right) z + 2z^{\mathrm{T}}\mathcal{P}\mathcal{B}u_{nl} + 2z^{\mathrm{T}}\mathcal{P}\mathcal{B}\Delta_t \\ &+ 2z^{\mathrm{T}}\mathcal{P}\mathcal{D}_1\Phi_1(z) + 2z^{\mathrm{T}}\mathcal{P}\mathcal{D}_2\Phi_3(z) \end{aligned} \tag{21}$$

Additionally, to ensure exponential stability, we will consider the subsequent condition:

$$\begin{aligned} \dot{\mathcal{V}}(z) + \eta\mathcal{V}(z) < 0 \quad &\text{such that} \quad -\sigma_{31} \leq \mathcal{C}^{\mathrm{T}} z \leq \sigma_{32} \\ &\text{and} \quad \|z\|^2 \geq \epsilon^2 \end{aligned} \tag{22}$$

with $\eta > 0$ denoting a predetermined positive scalar.

It follows that $\Phi_1(z)^2 = 1$ since $\Phi_1(z) = \mathrm{sgn}(\dot{\phi}) = \pm 1$. Consequently, utilizing the Young inequality [20], we derive the inequality:

$$2z^{\mathrm{T}}\mathcal{P}\mathcal{D}_1\Phi_1(z) \leq z^{\mathrm{T}}\mathcal{P}\mathcal{M}_1\mathcal{P}z + \mathcal{D}_1^{\mathrm{T}}\mathcal{M}_1^{-1}\mathcal{D}_1 \tag{23}$$

with $\mathcal{M}_1 = \mathcal{M}_1^{\mathrm{T}} > 0$.

Given that $\Phi_3(z)$ is a scalar function defined in (17), applying the Young's inequality yields:

$$2z^{\mathrm{T}}\mathcal{P}\mathcal{D}_2\Phi_3(z) \leq \tau_2 z^{\mathrm{T}}\mathcal{P}\mathcal{D}_2\mathcal{D}_2^{\mathrm{T}}\mathcal{P}z + \tau_2^{-1}\Phi_3(z)^2 \tag{24}$$

with $\tau_2 = \tau_2^{\mathrm{T}} > 0$.

It is straightforward to demonstrate that $\Phi_3(z)^2 = \cos^2(\theta_d) - 2\cos(\theta_d)\cos(\theta) + \cos^2(\theta)$. Then, considering that $\cos^2(\theta) \leq 1$ and $-2\cos(\theta) \leq a_2\theta + b_2$ with $a_2 = \frac{4}{\pi}$ and $b_2 = -2$, and let $\phi = \mathcal{C}_1 z$, where $\mathcal{C}_1 = \begin{bmatrix} 1 & 0 \end{bmatrix}$, we obtain:

$$\Phi_3(z)^2 \leq 2\mu_1\mathcal{C}_1 z + \mu_2 \tag{25}$$

with $\mu_1 = \frac{a_2}{2}\cos(\theta_d) > 0$ and $\mu_2 = 1 + a_2\cos(\theta_d)\theta_d + b_2\cos(\theta_d) + \cos^2(\theta_d)$.

Consequently, expression (24) may be written like this:

$$2z^{\mathrm{T}}\mathcal{P}\mathcal{D}_2\Phi_3(z) \leq \tau_2 z^{\mathrm{T}}\mathcal{P}\mathcal{D}_2\mathcal{D}_2^{\mathrm{T}}\mathcal{P}z + 2\mu_1\tau_2^{-1}\mathcal{C}_1 z + \mu_2\tau_2^{-1} \tag{26}$$

Moreover, since Δ_t is a scalar function and based on condition (5), applying the Young's inequality yields the subsequent inequality:

$$2z^{\mathrm{T}}\mathcal{P}\mathcal{B}\Delta_t \leq z^{\mathrm{T}}\mathcal{P}\mathcal{M}_3\mathcal{P}z + \bar{\delta}^2\mathcal{B}^{\mathrm{T}}\mathcal{M}_3^{-1}\mathcal{B} \tag{27}$$

with $\mathcal{M}_3 = \mathcal{M}_3^{\mathrm{T}} > 0$.

By substituting equations (23), (26), and (27) into inequality (21) and utilizing (22), we get the subsequent formulation:

$$\begin{aligned} \dot{\mathcal{V}}(z) + \eta\mathcal{V}(z) = z^{\mathrm{T}} &\Big((\mathcal{P}\mathcal{A} + \mathcal{P}\mathcal{B}\mathcal{K}) + (\mathcal{P}\mathcal{A} + \mathcal{P}\mathcal{B}\mathcal{K})^{\mathrm{T}} \\ &+ \mathcal{P}\mathcal{M}_1\mathcal{P} + \tau_2\mathcal{P}\mathcal{D}_2\mathcal{D}_2^{\mathrm{T}}\mathcal{P} + \mathcal{P}\mathcal{M}_3\mathcal{P} + \eta\mathcal{P} \Big) z + \mu_2\tau_2^{-1} \\ &+ \mathcal{D}_1^{\mathrm{T}}\mathcal{M}_1^{-1}\mathcal{D}_1 + 2\mu_1\tau_2^{-1}\mathcal{C}_1 z + \bar{\delta}^2\mathcal{B}^{\mathrm{T}}\mathcal{M}_3^{-1}\mathcal{B} + 2z^{\mathrm{T}}\mathcal{P}\mathcal{B}u_{nl} \end{aligned} \tag{28}$$

Next, we define the function $\lambda(z)$ as follows:

$$\lambda(z) = \mathcal{D}_1^{\mathrm{T}}\mathcal{M}_1^{-1}\mathcal{D}_1 + 2\mu_1\tau_2^{-1}\mathcal{C}_1 z + \mu_2\tau_2^{-1} + \bar{\delta}^2\mathcal{B}^{\mathrm{T}}\mathcal{M}_3^{-1}\mathcal{B} \tag{29}$$

In addition, let us look at the equation that represents the auxiliary nonlinear control law u_{nl}:

$$u_{nl} = \begin{cases} -\frac{1}{2}\frac{\mathcal{B}^{\mathrm{T}}\mathcal{P}z}{z^{\mathrm{T}}\mathcal{P}\mathcal{B}\mathcal{B}^{\mathrm{T}}\mathcal{P}z}\lambda(z) & \text{if} \quad \|\mathcal{B}^{\mathrm{T}}\mathcal{P}z\|^2 > \rho \\ -\frac{1}{2}\frac{\mathcal{B}^{\mathrm{T}}\mathcal{P}z}{\rho}\lambda(z) & \text{if} \quad \|\mathcal{B}^{\mathrm{T}}\mathcal{P}z\|^2 \leq \rho \end{cases} \tag{30}$$

with $\rho > 0$.

In the case when $\|\mathcal{B}^{\mathrm{T}}\mathcal{P}z\|^2 > \rho$, the inequality (28) may be simplified by replacing the nonlinear controller u_{nl} with the expression (30). This leads to:

$$\begin{aligned}\dot{\mathcal{V}}(z) + \eta\mathcal{V}(z) \leq z^{\mathrm{T}} \Big(&(\mathcal{P}\mathcal{A} + \mathcal{P}\mathcal{B}\mathcal{K}) + (\mathcal{P}\mathcal{A} + \mathcal{P}\mathcal{B}\mathcal{K})^{\mathrm{T}} \\ &+\mathcal{P}\mathcal{M}_1\mathcal{P} + \tau_2\mathcal{P}\mathcal{D}_2\mathcal{D}_2^{\mathrm{T}}\mathcal{P} + \mathcal{P}\mathcal{M}_3\mathcal{P} + \eta\mathcal{P}\Big) z \end{aligned} \tag{31}$$

However, as shown in (30), when $\|\mathcal{B}^{\mathrm{T}}\mathcal{P}z\|^2 \leq \rho$, the equation (28) is changed to:

$$\begin{aligned}\dot{\mathcal{V}}(z) + \eta\mathcal{V}(z) \leq z^{\mathrm{T}} \Big(&(\mathcal{P}\mathcal{A} + \mathcal{P}\mathcal{B}\mathcal{K}) + (\mathcal{P}\mathcal{A} + \mathcal{P}\mathcal{B}\mathcal{K})^{\mathrm{T}} \\ &+\mathcal{P}\mathcal{M}_1\mathcal{P} + \tau_2\mathcal{P}\mathcal{D}_2\mathcal{D}_2^{\mathrm{T}}\mathcal{P} + \mathcal{P}\mathcal{M}_3\mathcal{P} + \eta\mathcal{P}\Big) z \\ &+ \lambda(z)\left(1 - \frac{\|\mathcal{B}^{\mathrm{T}}\mathcal{P}z\|^2}{\rho}\right) \end{aligned} \tag{32}$$

Given that $\frac{\|\mathcal{B}^{\mathrm{T}}\mathcal{P}z\|^2}{\rho} \leq 1$, and assuming that $\lambda(z) > 0$, we can therefore conclude that:

$$\lambda(z)\left(1 - \frac{\|\mathcal{B}^{\mathrm{T}}\mathcal{P}z\|^2}{\rho}\right) \geq 0 \tag{33}$$

Consequently, according to the theorem of uniform ultimate boundedness [21], we verify that the specified $\mathcal{V}(z)$ in (18) stays limited. Thus, the trajectory within the closed loop stays bounded for any $\|\mathcal{B}^{\mathrm{T}}\mathcal{P}z\|^2 \leq \rho$. As a result, the only thing left to perform is to verify the condition (31).

B. LMI Conditions Development

The stability condition (31) can be recast like so:

$$\begin{bmatrix} z \\ 1 \end{bmatrix}^{\mathrm{T}} \begin{bmatrix} \Upsilon_{11} & \mathcal{O} \\ \star & \mathcal{O} \end{bmatrix} \begin{bmatrix} z \\ 1 \end{bmatrix} < 0 \tag{34}$$

with $\Upsilon_{11} = (\mathcal{P}\mathcal{A} + \mathcal{P}\mathcal{B}\mathcal{K}) + (\mathcal{P}\mathcal{A} + \mathcal{P}\mathcal{B}\mathcal{K})^{\mathrm{T}} + \mathcal{P}\mathcal{M}_1\mathcal{P} + \tau_2\mathcal{P}\mathcal{D}_2\mathcal{D}_2^{\mathrm{T}}\mathcal{P} + \mathcal{P}\mathcal{M}_3\mathcal{P} + \eta\mathcal{P}$. Note that here and in the sequel, the symbol $\star$ indicates an element's transposition. Furthermore, $\mathcal{O}$ and $\mathcal{I}$ represent the zero and identity matrices, with appropriate dimensions, respectively.

The constraints on the suggested Lyapunov function $\mathcal{V}(z)$, presented in (18), can be rephrased like this:

$$\begin{bmatrix} z \\ 1 \end{bmatrix}^{\mathrm{T}} \begin{bmatrix} \mathcal{O} & \mathcal{C} \\ \star & -2\sigma_{32} \end{bmatrix} \begin{bmatrix} z \\ 1 \end{bmatrix} \leq 0 \tag{35a}$$

$$\begin{bmatrix} z \\ 1 \end{bmatrix}^{\mathrm{T}} \begin{bmatrix} \mathcal{O} & -\mathcal{C} \\ \star & -2\sigma_{31} \end{bmatrix} \begin{bmatrix} z \\ 1 \end{bmatrix} \leq 0 \tag{35b}$$

$$\begin{bmatrix} z \\ 1 \end{bmatrix}^{\mathrm{T}} \begin{bmatrix} \mathcal{I} & \mathcal{O} \\ \star & -\epsilon^2 \end{bmatrix} \begin{bmatrix} z \\ 1 \end{bmatrix} \geq 0 \tag{35c}$$

Expressions (34) and (35) provide the basis upon which two distinct approaches to creating LMI-based stability criteria for the feedback gain $\mathcal{K}$ of the adopted controller, achieved using the following expression:

$$\mathcal{K} = \mathcal{R}\mathcal{S}^{-1} \tag{36}$$

1) First Approach for Formulating LMI Conditions: In our initial approach to designing the LMI conditions, we will concentrate on the nonlinear dynamics without incorporating state constraints [12], [13]. Our primary objective is to ensure the stability of the controlled robots using the extended expressions (34) and (35c). Subsequently, we will establish the following LMI constraint on the gain matrix $\mathcal{K}$ [20]:

$$\begin{bmatrix} \Xi_{11} & \mathcal{S} \\ \star & -\sigma_1\mathcal{I} \end{bmatrix} < 0 \tag{37}$$

where $\Xi_{11} = (\mathcal{A}\mathcal{S} + \mathcal{B}\mathcal{R}) + (\mathcal{A}\mathcal{S} + \mathcal{B}\mathcal{R})^{\mathrm{T}} + \mathcal{M}_1 + \tau_2\mathcal{D}_2\mathcal{D}_2^{\mathrm{T}} + \mathcal{M}_3 + \eta\mathcal{S}$.

Thus, we developed the LMI (37) that is constructed using the unknown matrix variables $\mathcal{R}$, $\mathcal{S}$, $\mathcal{M}_1$, and $\mathcal{M}_3$, and the unknown scalar variables σ_1, and τ_2.

2) Second Approach for Formulating LMI Conditions: In the second approach to developing the LMI conditions, we will address the nonlinear dynamics while considering state constraints [11], [22]. Our main goal will be to ensure the stability of the controlled robots by applying the extended expressions (34), (35a), (35b) and (35c). Subsequently, through mathematical manipulation and the use of technical lemmas, we will derive the following LMI conditions [20]:

$$\begin{bmatrix} \Xi_{11} & \mathcal{S} & -\frac{1}{2\sigma_{32}}\mathcal{S}\mathcal{C} & \frac{1}{2\sigma_{31}}\mathcal{S}\mathcal{C} \\ \star & -\sigma_3\mathcal{I} & \mathcal{O} & \mathcal{O} \\ \star & \star & \frac{\sigma_3}{\epsilon^2} - \frac{1}{2\sigma_{32}}\sigma_1 & \frac{\sigma_3}{\epsilon^2} \\ \star & \star & \star & \frac{\sigma_3}{\epsilon^2} - \frac{1}{2\sigma_{31}}\sigma_2 \end{bmatrix} < 0 \tag{38a}$$

$$\begin{bmatrix} -\frac{\sigma_3}{\epsilon^2} & -\frac{\sigma_3}{\epsilon^2} & -\frac{\sigma_3}{\epsilon^2} \\ \star & -\frac{1}{2\sigma_{32}}\sigma_1 & \mathcal{O} \\ \star & \star & -\frac{1}{2\sigma_{31}}\sigma_2 \end{bmatrix} < 0 \tag{38b}$$

with $\Xi_{11} = (\mathcal{A}\mathcal{S} + \mathcal{B}\mathcal{R}) + (\mathcal{A}\mathcal{S} + \mathcal{B}\mathcal{R})^{\mathrm{T}} + \mathcal{M}_1 + \tau_2\mathcal{D}_2\mathcal{D}_2^{\mathrm{T}} + \mathcal{M}_3 + \eta\mathcal{S}$.

Notice that the stability criteria represented by (38) corresponds to an LMI formulated with regard to unknown variables $\mathcal{S}$, $\mathcal{R}$, $\mathcal{M}_1$, $\mathcal{M}_3$, τ_2, σ_1, σ_2, and σ_3.

Remark 2: In this work, we proposed two LMI design approaches for determining feedback gains. The first approach, without state constraints, focuses on the nonlinear dynamics to ensure robot stability using extended equations (34). It is simpler to implement but may be limited in cases where state constraints are crucial. The second approach incorporates state constraints, offering a more general solution that ensures stability while respecting state limits (35). Although more complex, this method is essential for scenarios where safety or performance depends on maintaining specific state boundaries.

V. Simulation Outcomes

To validate the efficacy of the LMI requirements for stabilizing the knee-joint rehabilitation exoskeleton, we present some numerical and simulation results. The knee exoskeleton robot parameters presented in the dynamic model (1) are described in Table I. Numerical studies are conducted to validate the design strategy for the gain $\mathcal{K}$ in the adopted controller (14). For simulations, we select $\theta_d = 30^\circ$ as the target position for the knee exoskeleton. We provide an external disturbance Δ_t, which is characterized as a random signal that is active for a maximum of two to seven seconds.

$$\Delta_t = \bar{\delta} \times (2 \times \text{rand} - 1) \tag{39}$$

where rand generates a random signal between 0 and 1.

TABLE I

Values for the different parameters of the knee rehabilitation exoskeleton robot.

Par.	Value	Nom. Par.	Nom. Value	Unit
ϑ	0.323 + 0.1	$\vartheta_\star$	0.323	Kg.m^2/rad
m	0.1 +0.01	$m_\star$	0.1	Kg
l	0.25 + 0.05	$l_\star$	0.25	m
f_v	0.35 + 0.1	$f_v^\star$	0.35	N.m.s/rad
f_s	0.059 + 0.05	$f_s^\star$	0.059	N.m/A
g	9.8	-	-	N

A. Numerical Results

1) Numerical Results Obtained Utilizing the First Design Approach: In this part, we address the LMI problem using the first design approach. Resolving the LMI with fixed values $\bar{\delta} = 0.8$ and $\eta = 7$, we obtain:

$$\mathcal{K} = \begin{bmatrix} -48.3793 & -7.1431 \end{bmatrix} \tag{40}$$

2) Numerical Results Obtained Utilizing the Second Design Approach: In this part, we address the LMI problem using the second design method. With fixed values of $\bar{\delta} = 0.8$, $\epsilon = 1.2$ and $\eta = 2$, we achieve the following results:

$$\mathcal{K} = \begin{bmatrix} -11.0924 & -3.6381 \end{bmatrix} \tag{41}$$

B. Graphical Results

This section focuses on the second formulation method of the LMI condition, which yields smaller feedback gain $\mathcal{K}$, to present simulation results demonstrating the effectiveness of the adopted composite controller. We will present two simulation scenarios employing the proposed control law, starting from the same initial position and using the same desired position for the experiments. However, we will introduce two different types of external disturbances exerted on the knee exoskeleton robot. In the first simulation, an external disturbance Δ_t will be introduced as a random signal with $\bar{\delta} = 0.8$. In the second simulation, we will implement an external disturbance Δ_t represented by a sinusoidal input, with $\bar{\delta} = 3 \times 0.8$.

1) First Simulation: In the first simulation, an external disturbance Δ_t is introduced in the form of a random signal, defined by (39). Then, by selecting $\bar{\delta} = 0.8$, we obtained the graphical results shown in Fig. 2. These graphs illustrate the simulation outcomes in response to the disturbance torque Δ_t. The motion of the knee exoskeleton system exhibits fluctuations around its equilibrium point. As the effect of the disturbing torque diminishes, the knee exoskeleton robot stabilizes back to its intended position. These results confirm that the proposed composite controller effectively mitigates the disturbance, maintaining the knee exoskeleton system near its target position.

2) Second Simulation: In the second simulation, an external disturbance Δ_t is introduced as a sinusoidal input, described as follows:

$$\Delta_t = \bar{\delta} \times \sin(\omega_f \times t) \tag{42}$$

where here ω_f represents the angular frequency of the signal, set to $\omega_f = 10\pi$ in our case. This disturbance is active only between 2 and 7 seconds. For this simulation, we set $\bar{\delta} = 3 \times 0.8$, and obtained the graphical results shown in Fig. 3. These figures demonstrate that the exoskeleton robot was successfully controlled and reached the desired state. Additionally, the control effort u matched u_d when the exoskeleton robot stabilized at the intended position.

VI. Conclusion and Future Directions

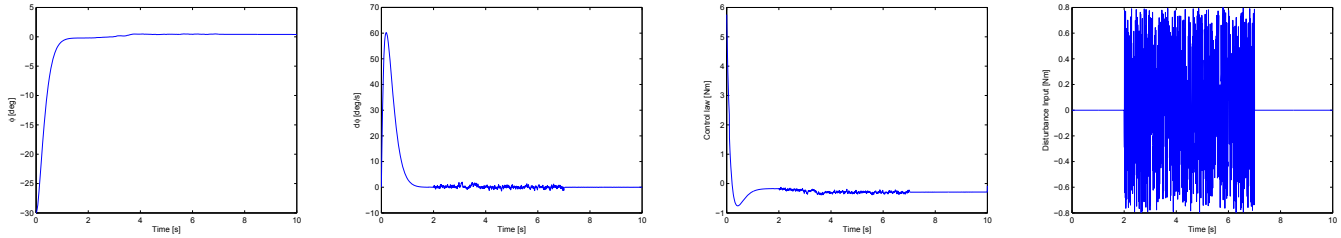
This study introduces a robust control system design for lower limb rehabilitation exoskeletons, focusing on enhancing physical reeducation for the elderly and pediatric therapy. We developed a composite controller that combines a linear state feedback controller with a nonlinear controller to manage the nonlinear dynamic model of the knee exoskeleton. The system addresses state constraints, parameter uncertainties, frictions, and external disturbances. Using a quadratic Lyapunov function, we establish LMI conditions for the gain of the controller through two design approaches. These conditions incorporate technical lemmas like the S-procedure, the Young inequality, the Schur complement, and the matrix inversion lemma. The controller's robustness is validated with external disturbances, and simulation results confirm its effectiveness in stabilizing the knee exoskeleton robot despite uncertainties and disturbances.

Our future goal is to explore alternative control strategies within the LMI framework, considering more complex uncertainty models to enhance the robustness of our methods. Furthermore, we aim to extend the design methodology to accommodate more complex lower limb rehabilitation exoskeletons with additional articulations and degrees of freedom.

References

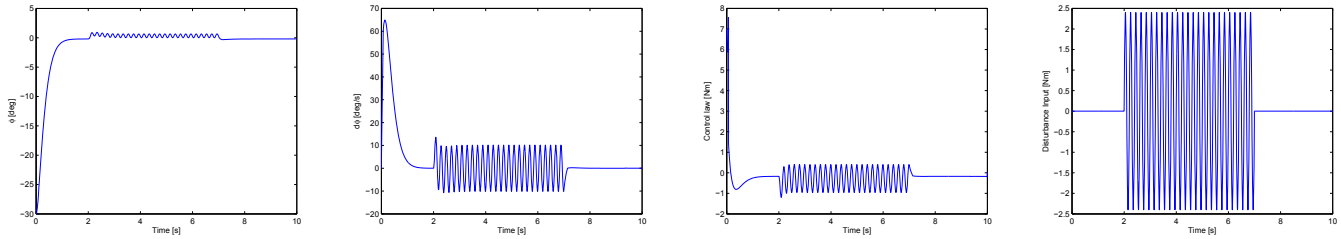
[1] D. Shi, W. Zhang, W. Zhang, and X. Ding, "A review on lower limb rehabilitation exoskeleton robots," *Chinese Journal of Mechanical Engineering*, vol. 32, no. 1, p. 74, 2019.

[2] B. Kalita, J. Narayan, and S. K. Dwivedy, "Development of active lower limb robotic-based orthosis and exoskeleton devices: a systematic review," *International Journal of Social Robotics*, vol. 13, pp. 775–793, 2021.



(a) (b) (c) (d)

Fig. 2. First simulation outcomes. Evolution of: (a) the angular position error ϕ, (b) the angular velocity error $\dot{\phi}$, (c) the proposed controller u, and (d) the external disturbance Δ_t.



(a) (b) (c) (d)

Fig. 3. Second simulation outcomes Evolution of: (a) the angular position error ϕ, (b) the angular velocity error $\dot{\phi}$, (c) the proposed controller u, and (d) the external disturbance Δ_t.

[3] J. Narayan and S. Kumar Dwivedy, "Preliminary design and development of a low-cost lower-limb exoskeleton system for paediatric rehabilitation," *Proceedings of the Institution of Mechanical Engineers, Part H: Journal of Engineering in Medicine*, vol. 235, no. 5, pp. 530–545, 2021.

[4] R. R. Torrealba, S. B. Udelman, and E. D. Fonseca-Rojas, "Design of variable impedance actuator for knee joint of a portable human gait rehabilitation exoskeleton," *Mechanism and Machine Theory*, vol. 116, pp. 248–261, 2017.

[5] J. Narayan, M. Abbas, and S. K. Dwivedy, "Robust adaptive backstepping control for a lower-limb exoskeleton system with model uncertainties and external disturbances," *Automatika*, vol. 64, no. 1, pp. 145–161, 2023.

[6] J. Narayan, H. Gritli, and S. K. Dwivedy, "Fast terminal sliding mode control with rapid reaching law for a pediatric gait exoskeleton system," *International Journal of Intelligent Robotics and Applications*, vol. 8, pp. 76–95, 2024.

[7] H. Rifaï, S. Mohammed, W. Hassani, and Y. Amirat, "Nested saturation based control of an actuated knee joint orthosis," *Mechatronics*, vol. 23, no. 8, pp. 1141–1149, 2013.

[8] M. Daachi, T. Madani, B. Daachi, and K. Djouani, "A radial basis function neural network adaptive controller to drive a powered lower limb knee joint orthosis," *Applied Soft Computing*, vol. 34, pp. 324–336, 2015.

[9] K. Suzuki, G. Mito, H. Kawamoto, Y. Hasegawa, and Y. Sankai, "Intention-based walking support for paraplegia patients with robot suit hal," *Advanced Robotics*, vol. 21, no. 12, pp. 1441–1469, 2007.

[10] K. Kong and M. Tomizuka, "Control of exoskeletons inspired by fictitious gain in human model," *IEEE/ASME Transactions on Mechatronics*, vol. 14, no. 6, pp. 689–698, 2009.

[11] S. Jenhani and H. Gritli, "Enhancing knee rehabilitation exoskeleton control via a robust LMI-based strategy and by considering state constraints," in *2023 IEEE 11th International Conference on Systems and Control (ICSC)*, 2023, pp. 905–911.

[12] S. Jenhani and H. Gritli, "An LMI-based robust state-feedback controller design for the position control of a knee rehabilitation exoskeleton robot: Comparative analysis," *Measurement and Control*, vol. 57, no. 9, pp. 1326–1346, 2024.

[13] S. Jenhani and H. Gritli, "Robust LMI-based state-feedback control of a knee exoskeleton robotic system," in *2023 20th International Multi-Conference on Systems, Signals & Devices (SSD)*, 2023, pp. 121–128.

[14] S. Jenhani, H. Gritli, and J. Narayan, "An LMI-based composite nonlinear controller design for robust stabilization of a knee rehabilitation exoskeleton robot," in *2024 10th International Conference on Control, Decision and Information Technologies (CoDIT)*, 2024, pp. 1430–1435.

[15] R. Bkekri, A. Benamor, M. A. Alouane, G. Fried, and H. Messaoud, "Robust adaptive super twisting controller: methodology and application of a human-driven knee joint orthosis," *Industrial Robot: the international journal of robotics research and application*, vol. 46, no. 4, pp. 481–489, 2019.

[16] Z. Wang, C. Yang, S. Zhang, S. Zhang, C. Yi, Z. Ding, B. Wei, and F. Jiang, "Knee flexion-assisted method for human-exoskeleton system," *IEEE Transactions on Neural Systems and Rehabilitation Engineering*, vol. 31, pp. 2800–2808, 2023.

[17] T. Madani, B. Daachi, and K. Djouani, "Adaptive controller based on uncertainty parametric estimation using backstepping and sliding mode techniques: application to an active orthosis," in *2014 European Control Conference (ECC)*, 2014, pp. 1869–1874.

[18] A. S. Aljuboury, A. H. Hameed, A. R. Ajel, A. J. Humaidi, A. Alkhayyat, and A. K. A. Mhdawi, "Robust adaptive control of knee exoskeleton-assistant system based on nonlinear disturbance observer," *Actuators*, vol. 11, no. 3, p. 78, 2022.

[19] S. Arof, E. Noorsal, S. Z. Yahaya, Z. Hussain, Y. Mohd Ali, M. H. Abdullah, and M. K. Safie, "Adaptive sliding mode feedback control algorithm for a nonlinear knee extension model," *Machines*, vol. 11, no. 7, 2023.

[20] H. Gritli and S. Jenhani, "LMI-based state feedback control of the underactuated inertia wheel inverted pendulum to the unstable upright position," *Journal of Vibration Testing and System Dynamics*, vol. 8, no. 2, pp. 207–234, 2024.

[21] S. Zhen, J. Hao, X. Liu, Q. Wu, H. Zhao, and Y.-H. Chen, "A practical robust bounded control for permanent magnet linear motor with inequality constraints," *Control Engineering Practice*, vol. 122, p. 105068, 2022.

[22] S. Jenhani and H. Gritli, "A robust LMI-based approach for the position control of a 1-dof knee rehabilitation exoskeleton robot considering state constraints," in *2024 IEEE International Conference on Interdisciplinary Approaches in Technology and Management for Social Innovation (IATMSI)*, vol. 2, 2024, pp. 1–6.